HCO rotational excitation in the photoinitiated unimolecular decomposition of H_2CO

M.J. Dulligan, M.F. Tuchler, J. Zhang [1], A. Kolessov, C. Wittig

Department of Chemistry, University of Southern California, Los Angeles, CA 90089, USA

Abstract

The unimolecular decomposition of H_2CO via the H + HCO radical channel has been examined by photoexcitation of the S_1 $2^2 4^3$ and $2^3 4^1$ vibrational bands (31500–31855 cm^{-1}). The H-atom translational energy distributions, obtained by using the high-n Rydberg time-of-flight technique, reflect the HCO internal energy distributions and reveal rotational excitation as high as $K_a = 6$ for $v = 0$. Such high-K_a levels are believed to be the result of contributions from the S_0 ground state surface at energies where the S_0 and T_1 radical pathways compete. © 1997 Published by Elsevier Science B.V.

1. Introduction

The formaldehyde molecule figures prominently in the history of the photochemistry and photophysics of small polyatomics. It has provided the first rotational analysis of the spectrum of a polyatomic molecule [1], the first viable means of laser isotope separation [2], and an excellent environment for examining radiationless decay processes [3], including unimolecular decomposition in the regime of quantum fluctuations [4–7]. Recent reviews provide ample background [8,9].

Fig. 1 shows several energies relevant to the present study, in which UV photoexcitation promotes molecules to the S_1 surface. The H_2 + CO molecular

channel proceeds from the S_0 ground state surface following $S_1 \rightarrow S_0$ internal conversion (IC), whereas the H + HCO radical channel involves both S_0 *and* T_1 surfaces, the latter following $S_1 \rightarrow T_1$ intersystem crossing (ISC). Because there is no barrier to radical products on S_0, reaction on this surface dominates over T_1 at threshold. On the other hand, at energies near the T_1 barrier the radical channel can proceed via S_0 and/or T_1, depending on the relative magnitudes of the S_1–S_0 and S_1–T_1 coupling matrix elements, proximities of S_1 and T_1 levels, tunneling probabilities on T_1, densities and widths of T_1 reactive resonances, etc.

An important factor that affects the respective participations of the S_0 and T_1 reaction pathways is the energy of the T_1 barrier. This is not known accurately, despite electronic structure calculations [10–12] and estimates based on experimental data [13]. In the tunneling regime below the top of the

---

[1] Present address: Department of Chemistry, University of California, Riverside, CA 92521, USA.
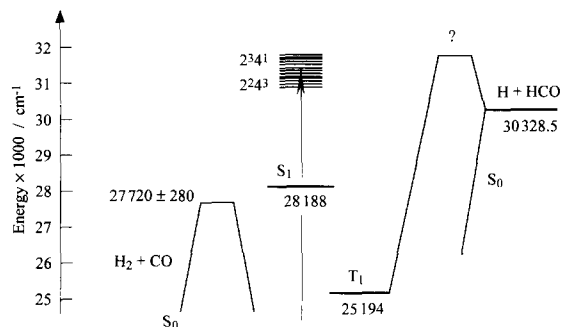
Fig. 1. Energy diagram showing features of the potentials relevant to the low-energy photochemistry; values listed include zero-point energies. $S_1 \rightarrow S_0$ internal conversion and $S_1 \rightarrow T_1$ intersystem crossing are both active. The energy of the T_1 barrier is not known accurately [10–13].

barrier, S_1–T_1 coupling is most efficient when the S_1 level lies close to the center of a T_1 resonance. In contrast, above the barrier the T_1 resonance widths are comparable to the mean spacing between the optically accessed T_1 resonances, and consequently the T_1 pathway is expected to dominate. However, the transition with increasing energy from S_0-dominance to T_1-dominance is complex.

In this Letter, we report HCO internal energy distributions obtained by using the high-n Rydberg time-of-flight (HRTOF) technique. Photon energies up to 31855 cm^{-1} have been used, and K_a levels up to 6 in the HCO ground vibrational level have been observed, with only $K_a = 0$ and 1 unresolved. For $K_a = 5$ and 6, the N-distributions display structure (N and K_a are quantum numbers for the angular momentum excluding spins and its projection on the a-axis, respectively, with HCO approximated by a
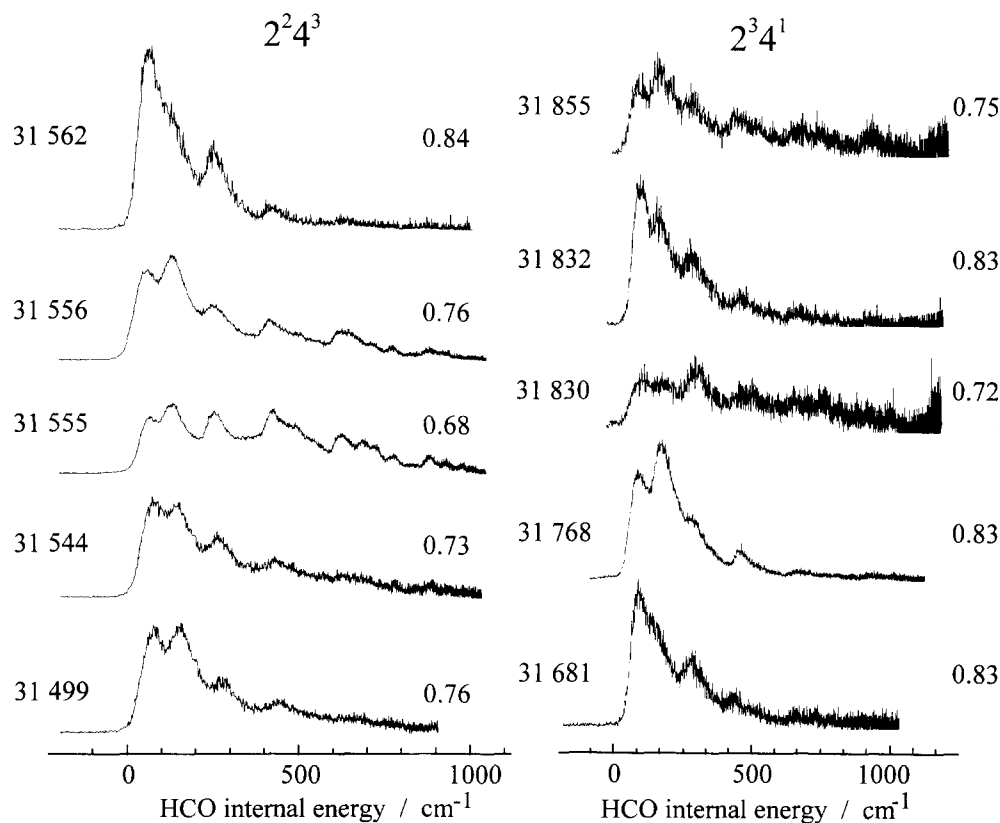

Fig. 2. Representative HCO internal energy distributions following $S_1 \leftarrow S_0$ photoexcitation of rotational levels within the $2^2 4^3$ and $2^3 4^1$ vibrational bands. The numbers to the left of the distributions are the photon wavenumbers. The fractions are upper bounds to the fraction of the available energy appearing as c.m. translation.

symmetric top). It is argued that the high-K_a levels arise from reaction via S_0, in which case the S_0 and T_1 reaction pathways may *both* be active.

2. Experimental

The experimental strategy is to use the HRTOF technique to record H-atom arrival time distributions, which are then transformed to center-of-mass (c.m.) translational energy distributions. Details are given elsewhere [14]. Note that since the H atoms are present only in their ground state, knowledge of the c.m. translational energy distribution is equivalent to knowledge of the HCO internal energy distribution, as given in Eq. (1):

$$h\nu + E_{int}(H_2CO) - D_0(H-HCO)$$

$$= E_{c.m.} + E_{int}(HCO) \qquad (1)$$

where $h\nu$ is the photolysis photon energy, $E_{int}(H_2CO)$ is the energy of the H_2CO S_0 rotational level that undergoes photoexcitation, $D_0(H-HCO)$ is the dissociation energy, $E_{c.m.}$ is c.m. translational energy, and $E_{int}(HCO)$ is the HCO internal energy. In the present study, HCO rotations are examined; H atoms corresponding to the bending mode (1081 cm^{-1}) are not detected due to their long arrival times.

A pulsed molecular beam of formaldehyde is generated by heating paraformaldehyde to $\approx 95°C$ in the delivery line, which contains ≈ 0.5 atm of Ne carrier. The gas mixture is expanded into the source chamber through a 0.75 mm diameter pulsed nozzle operating at 10 Hz with a pulse duration of 400 μs. T_{rot} is believed to be ≈ 10 K. The molecular beam is collimated by a 1 mm diameter skimmer located 2 cm from the nozzle, and the photolysis and probe laser beams intersect the molecular beam 5 cm downstream from the skimmer.

Tunable UV radiation for exciting H_2CO is obtained by frequency doubling the output of a Nd:YAG laser-pumped dye laser. Typically 10 mJ of ≈ 315 nm radiation (linewidth ≈ 0.12 cm^{-1}) is focused into the chamber by using a 1 m $f.l.$ lens. A time-of-flight spectrum is acquired for each laser firing. Spectra are averaged over $> 10^4$ such firings.

3. Results

Representative results from $S_1 \leftarrow S_0$ photoexcitation of rotational levels of the $2^2 4^3$ and $2^3 4^1$ vibrational bands are given in Fig. 2. An additional 20 distributions were recorded but are not shown. Two features of the data are clear: HCO is rotationally excited, and the rotational distributions change in an irregular manner with the photolysis photon energy. In addition, the fraction of the available energy partitioned into translation was analyzed and determined to be large (see below). Such behavior is found in all the distributions, independent of the vibronic bands excited.

The upper limit to the average fraction of the available energy partitioned into c.m. translation is approximately 0.75 (i.e., when all the spectra are considered together). This constitutes an upper limit because decay may occur for those metastable H atoms having long arrival times, and because there may be some contribution from the HCO bending mode, which is not detected in the present experiments.

Fig. 3 shows assignments which were made by approximating HCO as a prolate rotor. Since A, B and C are 24.1, 1.5 and 1.4 cm^{-1}, respectively [15], this approximation is adequate for the present study. These assignments are consistent with all of the distributions obtained in the present study.
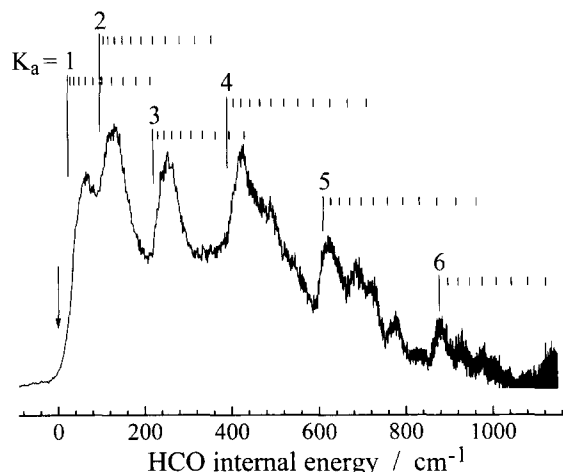

Fig. 3. Assignment for the distribution obtained with $h\nu = 31555$ cm^{-1}. The $K_a = 0$, $N = 0$ position is indicated by an arrow; $K_a = 0$ and 1 are not resolved. Note the structured N-distributions for $K_a = 5$ and 6.

4. Discussion

To achieve a quantitative understanding of the collision-free photoinitiated unimolecular decomposition of H_2CO via the radical channel, the roles of the energetically accessible potential surfaces, including couplings between them, must be established. In the present study, both the S_0 and T_1 surfaces are energetically accessible and offer competitive pathways for dissociation to radical products, as shown in Fig. 1.

Lifetimes of ≈ 5 ns have been measured for the S_1 $2^2 4^3$ and $2^3 4^1$ levels (without rotational resolution) and nonradiative decay rates of $\approx 2 \times 10^8$ s^{-1} have been inferred [16]. For single rotational levels, lifetime measurements have been reviewed [3] and general trends have been noted: (i) lifetimes vary erratically with rotational level, with the magnitude of this fluctuation decreasing with increasing E_{vib} and (ii) decay rates increase on average with E_{rot}.

For the analogous D_2CO system, it has been possible to examine S_0 levels at energies near the top of the $D_2 + CO$ barrier by using Stark level-crossing spectroscopy [4]. The $S_1 - S_0$ matrix elements obtained fluctuate as per the quantum-chaotic nature of the S_0 eigenstates, spanning the range $10^{-7} - 10^{-5}$ cm^{-1} [4] [2]. These results have been rationalized within the framework of quantum chaos by using a random matrix representation [17], and agreement with experiment is excellent.

4.1. The radical channel

As mentioned in the Introduction, at energies above the radical channel threshold (30328.5 ± 0.5 cm^{-1} [18]), there are contributions from both the molecular and radical channels [19]. Just above this threshold, only S_0 contributes to the radical channel since this path is barrierless, whereas there *is* a barrier on the T_1 path.

For energies not too far below the T_1 barrier, the radical channel may proceed from both the T_1 and S_0

surfaces. However, T_1 is expected to dominate at energies above the barrier [3]. Note that the unimolecular decomposition rate above the barrier on T_1 is orders of magnitude larger than the S_0 unimolecular decomposition rate at the same energy, due to the relatively low T_1 density of states. Thus, the rate-limiting step for the T_1 pathway is the transition from S_1 to T_1: if the system reaches T_1 it then evolves rapidly to products.

Accessing T_1 via $S_1 \leftarrow S_0$ photoexcitation requires ISC. This is known to occur in aldehydes [20], and $S_1 - T_1$ matrix elements have been estimated for H_2CO to lie between 0.01 and 0.1 cm^{-1} at the energies of the present study [21–23], making them much larger than the $S_1 - S_0$ matrix elements [4]. However, despite the fact that the unimolecular decomposition rates on T_1 are fast and the $S_1 - T_1$ matrix elements are much larger than the $S_1 - S_0$ matrix elements, it is not obvious a priori that T_1 dominates at the energies of the present experiments. This is due to the uncertainty of the energy of the T_1 barrier and poor overlap between S_1 levels and T_1 resonances in the tunneling regime below the barrier, as discussed below.

4.2. The energy of the T_1 barrier

Ramsey and coworkers [21–23] have carried out spectroscopic studies at energies up to the maximum used in the present study. Their results have been interpreted in terms of T_1 bound states and $S_1 - T_1$ matrix elements having values bracketed by the range 0.01–0.1 cm^{-1}. If this interpretation is correct, the T_1 barrier does not lie significantly below 31800 cm^{-1}.

Chuang et al. [13] conducted a detailed experimental study of the D + HCO and H + DCO radical channels of HDCO. Most importantly, the energy dependencies of the H/D ratio and the H(D) Lyman-α linewidth enabled them to comment on possible reaction mechanisms. They considered two limiting-case models in which the radical pathway switches

---

[2] Though $S_1 - S_0$ matrix elements have not been determined experimentally for H_2CO, calculations suggest that they are twice as large as for D_2CO (M.L. Elert, Ph.D. dissertation, University of California, Berkeley, 1977).

[3] Because $S_1 - T_1$ matrix elements are larger than $S_1 - S_0$ matrix elements, the T_1 pathway is expected to dominate when S_1 and T_1 levels are near-resonant. Broadening of T_1 resonances above the barrier facilitates meeting the resonance condition (Fig. 5).
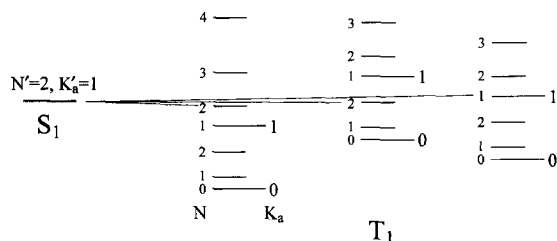
Fig. 4. This figure illustrates T_1 levels to which a given S_1 level can couple. The selection rules $\Delta N = 0$, ± 1, $\Delta K_a = 0$, ± 1, and $\Delta J = 0$ enable up to 9 T_1 levels to be accessed via a single S_1 level. Note that a given S_1 level can couple to only a single rotational level in a T_1 vibronic band because the spacings between rotational levels are large relative to the coupling matrix elements. Coupling to three such vibronic levels are shown.

from S_0 to T_1 with increasing energy: (i) Below the T_1 barrier, S_0 and T_1 compete (the latter reacting via a tunneling mechanism), whereas above the barrier, T_1 dominates completely. (ii) Switching from S_0 to T_1 is gradual, commencing at the barrier. In comparing these models to the data, it was concluded that the T_1 barrier lies between 2.9 and 6.0 kcal/mol (1020 and 2100 cm^{-1}) above H + HCO. Though these models do not provide the only possible rationalizations of the data, they are in accord with most of the known molecular properties in this energy region.

Following the above experimental studies, Schaefer and coworkers [12] calculated a value for the T_1 barrier of 7.8 ± 3 kcal/mol (2730 ± 1050 cm^{-1}) relative to H + HCO. If this is correct, S_0 can be expected to play at least some (and perhaps a significant) role in the photoinitiated reactions reported here. For example, their minimum value (i.e., the lowest permitted by the uncertainty) is 1680 cm^{-1}, which corresponds to 32010 cm^{-1} relative to the H$_2$CO ground state, using the recently determined value of D_0(H–HCO) [18]. This is higher than all of the energies of the present study. Thus, the most accurate calculation of the T_1 barrier to date is consistent with the barrier being higher than the energies of the present study, in agreement with the spectroscopic work of Ramsey and coworkers.

4.3. S_1–T_1 coupling

Stark level-crossing spectroscopy has been used to identify S_1–T_1 couplings in D$_2$CO [24]. Levels having triplet character were identified by splittings

which were induced by using a 100 Gauss magnet, and it was found that the number of observed transitions is in agreement with the S_1–T_1 selection rules $\Delta N = 0$, ± 1 and $\Delta K_a = 0$, ± 1 [25]. The S_1–T_1 coupling matrix elements limit the energy range over which coupling is effective. In the case of H$_2$CO, spacings between rotational energy levels within a given vibronic band are larger than these matrix elements. Thus, even though selection rules permit an S_1 level to couple to as many as 9 T_1 levels, only a single rotational level within any given T_1 vibronic level can be accessed. This is illustrated in Fig. 4.

Combining (i) the assumption that each H$_2$CO S_1 level is coupled to ≈ 9 T_1 levels (from the S_1–T_1 selection rules) with (ii) an estimated T_1 vibrational density of states of ≈ 0.3/cm^{-1} [4] yields ≈ 2.7 optically accessible states per cm^{-1}. Considering this, along with Ramsay and coworkers' estimated S_1–T_1 matrix elements, it is not surprising that S_1–T_1 perturbations were observed for only a modest percentage of the S_1 levels.

Now consider the tunneling regime. An important issue is the effectiveness of S_1–T_1 coupling as a function of parameters such as detuning from resonance, the dissociative widths of the T_1 levels $((\hbar \bar{\Gamma}_{T_1}))$, and the S_1–T_1 coupling matrix elements (V). For example, an S_1 level that is coupled to a single T_1 resonance (but not directly to the T_1 dissociation continuum) has a partial decay width [26]:

$$\hbar \Gamma_{S_1 \to T_1} = \frac{V^2 \hbar \Gamma_{T_1}}{\left(\dfrac{\hbar \Gamma_{T_1}}{2} \right)^2 + \left(E_{S_1} - E_{T_1} \right)^2} \qquad (2)$$

The average T_1 decay rate $(\bar{\Gamma}_{T_1})$ is taken as the transition state theory rate (k_{T_1}), and since the lowest frequency at the T_1 barrier is ≈ 500 cm^{-1} [12], only the first open channel needs to be considered here. In this case,

$$k_{T_1} = \frac{1}{h \rho_{T_1}} P \qquad (3)$$

where P is the tunneling probability.

---

[4] The T_1 vibrational state density was calculated by using experimental and ab initio values for the vibrational frequencies [12], which were taken as harmonic, with the exception that ν_4 excitation was computed from a fourth-order polynomial fit to the existing spectroscopic data [22].

Fig. 4 shows that a number of T_1 levels having different values of N and K_a can be accessed from a single S_1 level as per the S_1–T_1 selection rules. Though these N and K_a (on T_1) are not rigorous quantum numbers, if they are (approximately) conserved throughout the T_1 unimolecular decomposition process, then the T_1 levels accessed via S_1–T_1 coupling decay independently. We believe this to be the case, since reaction on T_1 is fast, as shown below.

Competition between the S_0 and T_1 pathways is reflected in the $S_1 \rightarrow S_0$ and $S_1 \rightarrow T_1$ partial widths, $\hbar \Gamma_{S_1 \rightarrow S_0}$ and $\hbar \Gamma_{S_1 \rightarrow T_1}$. Because of the sparse T_1 manifold and the upper and lower bounds on V (i.e., $0.01 \leq V \leq 0.1$ cm^{-1}), the possible values of $\hbar \Gamma_{S_1 \rightarrow T_1}$ span a large range. For example, with $\rho_{T_1} = 0.3/\mathrm{cm}^{-1}$ and assuming P = 0.5, Eq. (3) yields $k_{T_1} = 5 \times 10^{10}$ s^{-1}. The corresponding average width is $(\hbar \overline{\Gamma}_{T_1}) = 0.25$ cm^{-1}. Thus, for exact resonance, using $(\hbar \overline{\Gamma}_{T_1})$ in Eq. (2) yields: $1.6 \times 10^{-3} \leq \hbar \Gamma_{S_1 \rightarrow T_1} \leq 0.16$ cm^{-1}.

Alternatively, consider an off-resonance situation, e.g., $|E_{S_1} - E_{T_1}| = 1$ cm^{-1}, in which case Eq. (2) yields: $2.5 \times 10^{-5} \leq \hbar \Gamma_{S_1 \rightarrow T_1} \leq 2.5 \times 10^{-3}$ cm^{-1}. Thus, the role of ISC relative to IC might vary dramatically from one S_1 level to the next. Indeed, numerical experiments [5] show that a regime exists below the T_1 barrier in which there are pronounced state-to-state variations of the relative S_0 and T_1 contributions.

Above the T_1 barrier, the likelihood of overlap is good (Fig. 5), and the T_1 pathway is expected to dominate, though the S_0 pathway can still participate. In this regard, note that the molecular channel has been observed at energies up to 34000 cm^{-1} [3]. Since molecules that reach S_0 react via both the molecular and radical channels, the presence of the molecular channel suggests some contribution to the radical channel from the S_0 pathway.

4.4. Present results

Distributions such as those shown in Figs. 2 and 3 enable statements to be made concerning the roles of

Fig. 5. Schematic drawing showing S_1–S_0 and S_1–T_1 couplings below and above the T_1 barrier. Below the barrier, overlap between the S_1 level and the T_1 resonance plays a crucial role in determining the reaction pathway.

S_0 and T_1. For example, in Fig. 3 the HCO population extends to $K_a = 6$. Note that the energies of the $|1^0 2^0 3^0, N = 5, K_a = 5\rangle$ and $|1^0 2^0 3^0, N = 6, K_a = 6\rangle$ levels are 610 and 876 cm^{-1}, respectively, which are significant fractions of the energy available for product excitations (e.g., $h\nu - D_0 = 1226$ cm^{-1} for Fig. 3). Moreover, for both $K_a = 5$ and 6, the N-distributions on the high energy side of the $N = K_a$ positions display humps. From the spectrum alone, it is not possible to isolate those N values associated with a specific K_a, since the K_a stacks are not isolated. Nonetheless, the structure of the high-K_a features is unmistakable.

The high-K_a features are consistent with a decomposition mechanism that includes S_0. Though reaction via S_0 is barrierless, at the energies of the present experiments, the transition state is expected to tighten (i.e., move inward) relative to its location at lower energies [9], making a vibrational description of the open channels at the transition state appropriate. This has been confirmed for benchmark systems for barrierless unimolecular decomposition such as NCNO [27], NO_2 [28], and CH_2CO [9]. With this in mind, the high-K_a levels can be rationalized as being due to excitation of the out-of-plane bend mode at the transition state, which correlates to product orbital angular momentum and a-axis rota-

---

[5] Partial widths for S_1–T_1 coupling were calculated for the range 30300–32900 cm^{-1}, using random T_1 state energies, an average density of states of 2.7/cm^{-1}, and incorporating tunneling with a barrier of 32350 cm^{-1}.
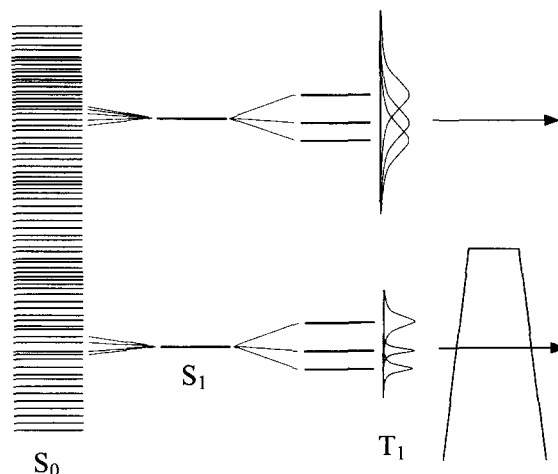
tion of HCO. Thus, the presence of high-K_a levels are consistent with an intuitive model of an S_0 transition state.

Transition state vibrational levels, when accessed randomly and projected into the product space, are also consistent with the structured N-distributions observed at $K_a = 5$ and 6. Such mappings, showing irregular distributions that depend sensitively on excitation wavelength, have been examined in detail for the case of NO_2 [28], and similar arguments apply here. However, we note that structured N-distributions can also be the consequence of high-N levels of one K_a stack extending into the next K_a stack. In this case, the structure is the result of the high-N levels being resolved. This issue requires further experimental work.

Reaction via T_1 is expected to display a significant propensity toward product c.m. translation due to the repulsive exit channel interaction between H and HCO. For energies near the top of the barrier, the HCO product is expected to have no vibrational excitation. In addition, rotational excitation is expected to be modest; due to the mass imbalance, exit channel repulsion between H and HCO is unable to apply sufficient torque to the HCO to induce significant rotational excitation. Thus, the low-K_a parts of the observed distributions are compatible with reaction via T_1, whereas the high-K_a parts are not. We also note that structured N-distributions are not expected for reactions via T_1 at energies near the top of the barrier.

The propensity toward product c.m. translation that is characteristic of a repulsive exit channel has been used to argue in favor of a T_1 mechanism [13]. However, because of the H/HCO mass imbalance, a propensity toward product c.m. translation will exist even for reaction via S_0, and this needs to be examined, including the variation of $\langle E_{trans} \rangle$ versus E_{excess} as HCO vibrational levels become energetically accessible.

5. Summary

The radical channel of photoinitiated H_2CO unimolecular decomposition has been examined by using the HRTOF technique to obtain c.m. translational energy distributions. From these, HCO rotational energy distributions have been obtained, and K_a levels have been identified up to $K_a = 6$. N-distributions for $K_a = 5$ and 6 display structure which may be due, at least in part, to accessing S_0 transition state levels whose mappings into the product space yield such distributions. The present results are interpreted as containing contributions from S_0. An accurate determination of the T_1 barrier would be most welcome.

References

[1] G.H. Dieke, G.B. Kistiakowsky, Phys. Rev. 45 (1934) 4.
[2] E.S. Yeung, C.B. Moore, Appl. Phys. Lett. 21 (1972) 109.
[3] C.B. Moore, J.C. Weisshaar, Annu. Rev. Phys. Chem. 34 (1983) 525.
[4] W.F. Polik, D.R. Guyer, C.B. Moore, J. Chem. Phys. 92 (1990) 3453.
[5] W.F. Polik, D.R. Guyer, W.H. Miller, C.B. Moore, J. Chem. Phys. 92 (1990) 3471.
[6] D.R. Guyer, W.F. Polik, C.B. Moore, J. Chem. Phys. 84 (1986) 6519.
[7] W.F. Polik, C.B. Moore, W.H. Miller, J. Chem. Phys. 89 (1988) 3584.
[8] W.H. Green Jr., C.B. Moore, W.F. Polik, Annu. Rev. Phys. Chem. 43 (1992) 591.
[9] C.B. Moore, I.W.M. Smith, J. Phys. Chem. 100 (1996) 12848.
[10] W.H. Fink, J. Am. Chem. Soc. 94 (1972) 1073.
[11] D.M. Hayes, K. Morokuma, Chem. Phys. Lett. 12 (1972) 539.
[12] B.F. Yates, Y. Yamaguchi, H.F. Schaefer III, J. Chem. Phys. 93 (1990) 8798.
[13] M.C. Chuang, M.F. Foltz, C.B. Moore, J. Chem. Phys. 87 (1987) 3855.
[14] J. Zhang, M. Dulligan, C. Wittig, J. Phys. Chem. 99 (1995) 7446.
[15] J.W.C. Johns, A.R.W. McKellar, M. Riggin, J. Chem. Phys. 67 (1977) 2427.
[16] R.G. Miller, E.K.C. Lee, J. Chem. Phys. 68 (1978) 4448.
[17] W.H. Miller, R. Hernandez, C.B. Moore, W.F. Polik, J. Chem. Phys. 93 (1990) 5657.

[18] A.C. Terentis, S.H. Kable, Chem. Phys. Lett. 258 (1996) 626.

[19] K.Y. Tang, P.W. Fairchild, E.K.C. Lee, J. Phys. Chem. 83 (1979) 569.

[20] A.C. Terentis, P.T. Knepp, S.H. Kable, J. Phys. Chem. 99 (1995) 12704.

[21] C.M.L. Kerr, D.C. Moule, D.A. Ramsay, Can. J. Phys. 61 (1983) 6.

[22] D.J. Clouthier, D.A. Ramsay, Annu. Rev. Phys. Chem. 34 (1983) 31.

[23] D.A. Ramsay, S.M. Till, Can. J. Phys. 57 (1979) 1224.

[24] W.F. Polik, Ph.D. dissertation, University of California, Berkeley, 1988.

[25] W.E. Howard, E.W. Schlag, J. Chem. Phys. 68 (1978) 2679.

[26] C. Cohen-Tannoudji, J. Dupont-Roc and G. Grynberg, Atom-Photon Interactions (Wiley, New York, 1992) p. 59.

[27] S.J. Klippenstein, L.R. Khundkar, A.H. Zewail, R.A. Marcus, J. Chem. Phys. 89 (1988) 4761.

[28] S.A. Reid, H. Reisler, J. Phys. Chem. 100 (1996) 474.